General Characteristics of Stratospheric Singular Vectors

Ronald M. Errico[1,2]

Ronald Gelaro[2]

Elena Novakovskaia[3,2]

Ricardo Todling[4,2]

Submitted to *Meteorologische Zeitschrift*

28 February 2007

[1] Goddard Earth Science Technology Center, University of Maryland Baltimore County

[2] Global Modeling and Assimilation Office, Goddard Space Flight Center

[3] Earth Resources Technology, Inc.

[4] Science Applications International Corporation

Corresponding author's address: Ronald M. Errico, Global Modeling and Assimilation Office, NASA/GSFC Code 610.1, Greenbelt, MD 20771. Email: rerrico@gmao.gsfc.nasa.gov

Abstract

Leading singular vectors have been computed for a numerical weather prediction model that can resolve dynamical structures within the stratosphere and lower mesosphere. The norm applied at the final time is the commonly used energy norm but confined to measuring the stratosphere. These stratospheric singular vectors are described by presenting three examples. They are produced using either of two initial norms that weight perturbations within the troposphere versus stratosphere very differently. For either initial norm, singular values are typically smaller than their tropospheric counterparts and they are less geographically local. They also retain their relevance to corresponding nonlinear evolutions for longer periods and larger amplitudes. For these reasons, stratospheric SVs may be useful for explaining observed stratospheric dynamical behaviors.

1. Introduction

The examination of atmospheric singular vectors (SVs) has fostered new insights into tropospheric dynamics and the behavior of short-term, forecast error growth (Farrell, 1989; Buizza and Palmer, 1995; Ehrendorfer and Errico, 1995; Buizza et al., 1997; Palmer et al., 1998; Gelaro et al., 2000; Reynolds et al., 2001). Until now, attention has focused on the troposphere, motivated by applications in numerical weather prediction (NWP) and due to limitations in older models for which adjoints were available. These limitations included low stratospheric resolutions, strong, artificial stratospheric "sponges" to filter amplifying vertically propagating waves, and a common numerical need to restrict measuring norms to the troposphere.

There are many questions concerning stratospheric dynamics for which singular vectors may also provide fresh insights. These concern the genesis of sudden warmings and the nature of interactions with the troposphere (Andrews et al., 1987). Stratospheric dynamics are often described in terms of waves and quasi-linear behaviors, suggesting that tangent-linear SVs may be particularly useful for stratospheric applications. Since highly nonlinear boundary layer and precipitation–generating processes play little role at high altitudes, it is possible that the tangent linear approximation upon which SVs are based will hold even better than in the troposphere.

In this first examination of stratospheric SVs at the U.S. National Aeronautics and Space Administration (NASA), rather than jump to a specific stratospheric question, the general characteristics of these SVs are examined. In particular, the several ways in which they are dramatically different than their tropospheric cousins are noted. Also, additional issues that must be considered regarding the choices of norms are described.

Aspects of the NASA model that are particularly relevant to SV determination are

presented in the next section. The norms used to determine the SVs are defined in section 3 followed in section 4 by a brief description of the reference state for the period forming the focus of this presentation. The leading SVs determined for the two norms during this focus period are described in sections 5–6 along with a noteworthy one for an earlier period. Comparisons of tangent linear and nonlinearly evolved perturbations initialized using these SVs appear in section 7, followed by a summary.

2. Model

The NASA model used here is the Goddard Earth Observing System (GEOS–5) general circulation model with the finite–volume dynamical core developed by Lin and Rood (1996). The model has a hybrid (mixed, terrain–following, standard σ and constant pressure) vertical coordinate defined on 72 levels, with those above 150 hPa (model level index $k = 40$, counting from the top) being constant pressure surfaces. The spacing of the levels is further described in the next section and the model top (p_t) is at 0.01 hPa. The model filters tendencies having short longitudinal scales near the poles in order to avoid the very short time steps otherwise required. Attached to the dynamics are parameterizations for all the standard physical processes found in most general circulation and NWP models.

The tangent linear version of the dynamics is exact, but a minimal set of simplified linearized physics has been added. This includes standard second–order, temporally semi–implicit, vertical diffusion applied throughout the depth of the atmosphere, with the diffusion coefficients defined at each time step by those in the reference trajectory forecast about which the linearization is performed. No perturbations of these coefficients are considered, however, to ensure numerical stability of this linearized version. This scheme includes surface momentum drag with a coefficient that is determined from the reference state using the surface physics in the nonlinear model. There is no linearized surface temperature flux

2

term. The tangent linear version also includes a semi–implicit, fourth–order horizontal diffusion scheme. There is no such scheme in the nonlinear model because, apparently, the nonlinear finite–volume algorithm, along with the time filtering of tendencies near the poles, provides enough spatial smoothing.

Additionally, a damping factor ν_k is applied to the tangent linear u', v' and T' fields above 70 hPa at each time step after the field is updated by the dynamics and other physical tendencies, where

$$\nu_k = \exp\left[-\frac{\Delta t}{c_1}\left(\frac{c_1}{c_{k_m}}\right)^{\frac{k-1}{k_m-1}}\right] ,$$

with $k = 1, \ldots, k_m$ being the levels over which the sponge is applied, Δt being the physics time step (1800 s here), and c_1 and c_{k_m} corresponding to the minimum and maximum e-folding damping times of 0.7 days and 30. days, respectively. This term is intended to represent effects of the nonlinear model's sponge applied to all fields in the mesosphere as well as effects of radiative cooling in the stratosphere.

The adjoint model is exact with respect to the tangent linear model, such that its resolvent matrix is an exact transpose (Errico 1997). The time steps used in the nonlinear, tangent linear, and adjoint models are identical. Trajectory information is stored for every time step, and no additional approximations to the time scheme are made for linearization.

3.   Norms

There are two norms considered for this study. One is the commonly used, total energy norm (Talagrand, 1981; Errico, 2000a):

$$E = \frac{1}{2}\sum_{i,j,k} \Delta A_j \Delta\sigma_{i,j,k}\left(u'^2 + v'^2 + aT'^2 + bp_s'^2\right) , \qquad (1)$$

3

where u', v', T', and p'_s are perturbation wind components, temperature, and surface pressure fields with understood longitude, latitude and vertical indexes i, j, k, respectively, where appropriate, and ΔA_j is a fractional surface area for each horizontal grid point. The weights $a = C_p/T_r$ and $b = RT_r/p^2_{sr}$, with c_p being the specific heat of air, R the gas constant, and T_r and p_{sr} prescribed, location-independent (e.g., mean) values of temperature and surface pressure. Values of $T_r = 280$ K and $p_{sr} = 1000$ hPa are used, yielding $a \approx 3.59$(J/kg)/K^2 and $b \approx 8 \times 10^{-6}$(J/kg)/Pa^2. The vertical weight $\Delta\sigma_{i,j,k} = \Delta p_{i,j,k}/(p_{s\ i,j} - p_t)$ is computed for each layer of pressure "thickness" Δp within each column using the values obtained from the reference trajectory at the times the norm is computed.

This E may also be considered a combined measure of the mean squares of u', v', T' and p'_s using fractional mass as a vertical weight. Note that above 150 hPa where the model levels are isobaric surfaces, this vertical weight tends to be larger over high topography where p_s is small (by as much as a factor of 2 over Tibet). Near the surface, however, where the vertical coordinate is purely terrain following, all geographic regions are almost equally weighted. For a more lengthy discussion of the properties and interpretation of this norm, see Errico (2000a).

The motivation for another norm is described in section 6. This second norm is given by

$$V = \frac{1}{2} \sum_{i,j,k} \Delta A_j \Delta z_{i,j,k} \left(u'^2 + v'^2 + aT'^2 + bp'^2_s \right) . \tag{2}$$

It is identical to the E norm except that $\Delta\sigma_{i,j,k}$ is replaced by

$$\Delta z_{i,j,k} = \Delta \ln p_{i,j,k}/(\ln p_{s\ i,j} - \ln p_t) , \tag{3}$$

where Δz is the difference in $\ln p$ between the two interfaces sandwiching each layer. If the temperature throughout a column of air were constant, Δz would be proportional to

4

the spatial thickness of a layer. The denominator in (3) is included so that, as for $\Delta\sigma$, the vertical weights sum to 1. Analogous to E, the V norm may also be considered a combined mean square of the fields, but with a fractional distance rather than fractional mass as the vertical weight. It also will tend to weight the norm over high topography more than low, but by a factor less than approximately 1.06 at $p_s = 500$ hPa. The possible need for this new norm is also discussed in Lewis et al. (2001).

Values of $\Delta\sigma$ and Δz for the particular reference–state value $p_s = 1000$ hPa are presented in Fig. 1. The $\Delta\sigma$ are a maximum near 300 hPa with values a factor of 3.3 smaller near the surface. Above 300 hPa, however, they rapidly decay approximately exponentially so that the ratio of values at 500 hPa and 0.1 hPa is 1200. In contrast, for 0.1 hPa$< p <$500 hPa, Δz varies by less than a factor of 5. Values of Δz below 800 hPa are approximately 10 times smaller than those near the tropopause.

At the final time, only a form of the E norm is applied in all the experiments. It differs from (1) in that it is only applied to a region of interest, specified here as 30°N – 90°N and 10 hPa – 90 hPa ($15 \leq k \leq 37$). The normalizations of $\Delta\sigma$ and A are recomputed for this application so that both sum to 1 over the specific region of interest. This localization of the norm does not constrain the evolved SV at final time to lie wholly within this region but does mean that only the portion of its structure that is within this region is measured by the norm and thus is considered by the optimization problem defining the SVs. At the initial time, either the E or V norm is applied, with both computed globally. The SVs are determined using 12 or more iterations of a Lanczos algorithm such that the first few squared singular values and singular vectors appear to be converged.

4.   Reference states

The reference states for which the SVs are computed are determined by 5–day forecasts begun from analyses produced using the GEOS–5 data assimilation system. Observations directly affecting the stratosphere include satellite–observed radiances and, at only low altitudes, a few rawindsondes. The analysis and subsequent nonlinear forecasts used to define the evolving state are produced at a horizontal resolution of 1° latitude by 1.25° longitude. The tangent linear and adjoint versions, however, are produced at a resolution of 4.5° latitude by 5° longitude. This low resolution appears sufficient based on the rather large scales of the SVs that have been produced.

SVs were computed for 34 periods throughout the summer of 2005 and the following winter. Attention in this report is primarily focused on the single 5–day period of 21–26 January 2006, beginning 0 UTC. During this focus period, a dramatic sudden warming occured in the winter polar stratosphere. The 50 hPa temperature at the North Pole rose by approximately 20°C and the zonal–mean zonal winds at 60°N for 10 hPa and 5 hPa became easterly and vanished, respectively. Results for other periods are mentioned here only for the purpose of supporting the generality of the presented results and revealing some ranges of behaviors.

Although not assured a–priori, the 5–day, model–produced reference forecast for the focus period also reveals a dramatic sudden warming. The initial and final 50 hPa geopotential height fields between 20°N and the North Pole appear in Fig. 2. At first glance, the initial pattern may be characterized as a single polar vortex centered just north of Scandinavia, with a notable smaller scale trough reaching into central Russia. The initial heights at the center of the vortex and at the North Pole are 1940 dm and 1975 dm, respectively. After 5 days, the single vortex is replaced by a wavenumber 3 (or larger scale) pattern,

6

with large scale troughs just west of the Ural Mountains, over Northern Siberia, and over the Queen Elizabeth Islands, and two smaller scale troughs embedded in the latter. At this time, the height at the pole is 2005 dm and the lowest height within the region shown is 1955 dm. At 60°N, the mean height gradient and thus zonal mean geostrophic wind are dramatically smaller than initially.

5.   Properties of E norm SVs

The leading squared singular values determined for individual 5–day periods sampled for the winter period November 2005 through February 2006 computed using the E norm range between 155 and 12. These values are the factor by which E increases during the 5–day periods. For the focus period, this factor is 64.

For the focus period, the vertical integral of the contribution to E at each horizontal grid point is shown in Fig. 3 for the leading SV at both initial and final times. Note that these values are spread over a much greater geographical area than is typical for leading tropospheric E–norm SVs (Buizza et al., 1997; Gelaro et al., 2000; Reynolds et al., 2001). In fact, when such non–local leading tropospheric SVs are obtained, the result almost always indicates non–convergence of the Lanczos algorithm used to obtain the solutions. Experiments conducted to explore this issue will be described later in this section. At the initial and final times, the fractions of E contributed by kinetic energy are 0.51 and 0.65, respectively. The wind perturbations are almost entirely nondivergent at both times. Leading tropospheric E norm SVs typically have smaller kinetic energy fractions than this at their initial times but larger fractions at their final times.

The horizontal integral of the contributions to E at each model level appear in Fig. 4a. The labeled ordinate is the level's pressure presented on a logarithmic scale, with values

for hybrid–defined coordinate levels specified by assuming $p_s = 1000$ hPa. The two curves are for initial and final times, with each curve normalized such that its sum over all model levels is 1. Note that the E contributions are largest near 20 hPa at both times, with very little contributions from the troposphere. Thus, this SV appears to describe a growing non–modal structure essentially confined to the stratosphere. This stratospheric confinement is a common feature of the leading E–norm SVs produced for all the winter 5–day periods examined.

Plots of the contribution to E by each model level (or layer) as in Fig. 4a can be misleading. For example, if the horizontally mean squared value of u'^2 in each layer were the same, contributions to E can still vary greatly in the vertical unless $\Delta\sigma$ is identical for each layer. In this model, $\Delta\sigma$ varies greatly as shown in Fig. 1, as it must for all NWP models that attempt to simultaneously model the troposphere, stratosphere, and lower mesosphere. So, a presentation as in Fig. 4a can be revealing more about the grid structure of the model than about its dynamics. An analogous warning about interpretations of vertical distributions for adjoint model results is presented in Lewis et al. (2001).

For the above reason, the vertical distribution of E is instead presented as an energy density in Fig. 4b. This is $E/\Delta\sigma$ computed for each level. This may also be interpreted as a weighted sum of the horizontal mean squares of the perturbations over all model levels and fields. It reveals that the largest values occur for $p < 1$ hPa at both times rather than near 20 hPa. The dramatic change in the presentation occurs because at this height in the model atmosphere, the spacing of the levels is approximately equal in $\Delta \ln (p)$, so that $\Delta\sigma$ decreases nearly exponentially with decreasing p. The vertical distribution of E in Fig. 4a is in large part due to this distribution of model layer thicknesses. The vertical weighting determined by this vertical spacing has other implications as well that will be presented in the following section.

Cross sections of v' at initial and final times appear in Figs. 5a,b, respectively. These are along 60°N and 75°N, respectively, where magnitudes of the fields are large. Note the strong westward tilt with increasing height at the initial time. This is an even more extraordinary tilt than typically obtained for tropospheric SVs (e.g., as discussed in Hoskins et al., 2000). In strong contrast, at final time the SV has much less tilt, analogous to the lessening of tilt obtained as typical tropospheric SVs evolve (e.g., Gelaro et al., 2000).

In the remainder of this section, the leading E–norm SV for the period is described for the purpose of revealing additional aspects of the non–local nature of the stratospheric SV structures. The initial horizontal distribution of vertically–integrated E appears in Fig. 6a. Note that it is highly nonlocal with three centers of activity: over Eastern Canada, the North Atlantic, and Siberia. To investigate whether these should actually be associated with distinct SVs and appear combined here only due to non–convergence of the Lanczos algorithm used to determine the SVs, this particular SV has been dissected into three components using the partitioning along the meridians indicated in the figure. Each component includes all fields at all levels in the indicated sector. Since the distribution and especially distinctiveness of local maxima or minima at individual levels for individual initial fields may dramatically differ from the integrated E shown in Fig. 6a, this specific dissection is therefore somewhat arbitrary. The dissection is only applied to create three distinct and uncorrelated initial conditions that are each then evolved independently using the tangent linear model.

The 5–day evolved u' field at 10 hPa begun from the sectors labeled 1–3 appear in Figs. 6b–d, respectively. The three separate sections apparently produce highly correlated results. Area–weighted correlations for the 10 hPa u' fields north of 30°N are 0.80 for results produced from sectors 1 and 2, 0.89 for 1 and 3, and 0.59 for 2 and 3. These values are typical of corresponding u', v', and T' results at all levels within the domain over which

the final E norm is measured. Thus, although initially well separated, the three evolutions produce solutions that reinforce each other when added. The SV that optimizes E at the final time given a constrained value of E at the initial time will therefore necessarily include initial contributions by all three sectors, for the general reason described by Errico (2000b). This is analogous to the combining of rotational and gravitational components to yield optimal E–norm growth for tropospheric SVs (Errico, 2000b). The nonlocalness is therefore due to the dynamics that render the distinct evolved results so similar rather than evidence of non–convergence of the Lanczos algorithm. This conclusion was confirmed by doubling the number of Lanczos iterations to check that the additional iterations negligibly affected the structure of the leading SV.

6. Properties of V–norm SVs

An effect of the spacing of the model's vertical grid on interpreting the E norm was presented in the last section, however, it also profoundly affects the structures determined by the SV optimization problem. Maximizing the ratio of E at the final time compared with its value at the initial time concerns not only maximizing the final value but also minimizing the initial one. The value of E at the initial time can be considered a penalty. Since the E norm gives much more weight to tropospheric levels than to stratospheric or mesospheric ones, it effectively penalizes the placement of initial perturbations in the lower atmosphere. For example, $\Delta\sigma$ at 500, 50, and 5 hPa are respectively 0.043, 0.009, and 0.001. Placing a mean value of u'^2 at 500 hPa therefore creates 43 times the penalty of doing the same at 5 hPa. As long as the dynamics can yield enough growth for a perturbation placed at higher levels, the smaller penalty for initially placing perturbations there can outweigh a weaker dynamical response.

In the previous section, the E norm SVs were revealed to be essentially confined to the

stratosphere. In light of the caveat above, it is therefore appropriate to ask if this general result is revealing more about the model's vertical grid structure or about stratospheric dynamics. For this reason, SVs were also produced using the V norm at the initial time. At the end time, the E norm confined to the stratosphere was still used, so that the squared singular values therefore equal the ratios of final stratospheric E to initial V. As revealed in Fig. 1, these new SVs will penalize tropospheric variances less severely compared to their stratospheric or mesospheric counterparts.

The fractional contributions to E at each model level and the corresponding energy densities for this V–norm SV appear in Fig. 7. These values are very unlike those in Fig. 4 for the E norm. For the V norm initially, 80% of the E is located below 500 hPa, with its maximum at 790 hPa. At the final time, the maximum occurs at 300 hPa with a much smaller secondary peak in the stratosphere. Only 13% of E is in the stratospheric layers where it is considered in determining the ratio E/V to be maximized for defining the leading SV. The energy densities (Fig. 7b) are even more dominant in the lower troposphere, where $\Delta\sigma$ is defined to be small. With its reduced penalty on initial tropospheric perturbations, the initial SV produced for the V norm is predominately tropospheric. Presumably, the tropospheric dominance at the final time is simply due to the large initial values at those levels, since the optimization problem defining the SV does not explicitly consider the final tropospheric fields.

For the initial V–norm SV, examination of cross sections (not shown here) through the lower troposphere where its fields have local maxima reveal tilts more like those observed for leading tropospheric SVs than as appearing in Fig. 5. This result, and comparison of Figs. 7 and 4 suggests that the V– and E–norm SVs bear little resemblance to each other. Examination of their corresponding horizontal fields at each model level, however, reveals remarkable similarities in the shapes of structures. This is confirmed in Fig. 8 where the

11

horizontal correlations of corresponding u' and T' fields at individual model levels for the two SVs are shown for both initial and final times. At the initial time for both u' and T', correlations are above 0.8 except in the mid–stratosphere. At the final time they are between 0.6 and 0.8 at almost all levels. So, the change of vertical weights (between the E and V norms) has primarily changed the amplitudes of the SV structures at each level rather than the shapes of the structures within each level.

7. Relevance to nonlinear evolution

Since SVs are determined based on linearized dynamics, if their relevance is to be claimed in the nonlinear context as well, evidence must be offered. This relevance can depend critically on amplitudes, time periods, synoptic situations, and metrics (Errico et al., 1993), and thus is difficult to state generally, without regard to any specific application. Here, the time period and synoptic situation are given by those that define the SVs and the metrics are correlations and final maximum magnitudes of the perturbation fields (Errico and Raeder, 1999, Reynolds and Rosmond, 2003).

For the test here, the initial magnitudes of the SV structures used to create differences in the nonlinear forecasts have been chosen by simply multiplying the initial E or V norm SVs by a scalar factor of 0.1. For the E norm SVs, this yields maximum initial magnitudes of u', v', and T' equal to 16 ms^{-1}, 7 ms^{-1}, and 3.6 K, respectively. All of these maxima are located in the upper stratosphere or lower mesosphere. These rather large amplitudes were investigated because they yielded final–time perturbations having magnitudes similar to the temporal changes occurring in the nonlinear reference forecast over five days, and thus may be of interest in future examinations of the stratospheric sudden warming problem. For the E norm, the maximum initial wind perturbations are less than 0.1 ms^{-1} below 500 hPa.

Representative stratospheric fields for the leading evolved E norm SV at day 5 for the focus period are presented in Fig. 9. Specifically, these are u' at 10 hPa (Figs. 9a,c) and T' at 50 hPa (Fig. 9b,d). The tangent linear evolution of the perturbation appears in Figs, 9a,b and the corresponding differences between the perturbed and reference nonlinearly evolved solutions appear in Figs. 9c,d. The latter are computed using the model with its complete physics package, so the comparison concerns not simply dynamical nonlinearity but also the faithfulness of the greatly simplified physics included in the tangent linear and adjoint models with respect to the complete nonlinear model.

For the nonlinear difference fields shown in Fig. 9, the maximum absolute values for u' and T' are 49 ms^{-1} and 8.4 K, respectively, with corresponding values less than 10% lower for the tangent linear result. The correlations between the two u' fields is 0.66 and for T', 0.82. This is remarkable agreement given the large perturbation magnitudes and long time period examined.

The horizontal correlations for u', v', and T' at all levels for the above experiment appear in Fig. 10a. Near 50 hPa, the correlations for all fields are larger than 0.7. Within the stratosphere, the correlations generally drop as levels for successively lower $p < 50$ hPa are considered. In the troposphere, the correlations for all fields are below 0.3. The result that local maxima or minima in the horizontal correlations for T' appearing in Fig. 10a occur closely below those for winds is related to the fact that winds at any level are hydrostatically and geostrophically related only to the temperatures at and primarily below that level. The maximum absolute magnitudes for the nonlinearly determined perturbations at levels $p < 1$ hPa are slightly larger than the corresponding linear results, but within the troposphere, these magnitudes are typically ten times larger than their tangent linear values. For this SV with this initial magnitude, the tropospheric portions of the tangent linear solutions are therefore unreliable in the nonlinear context.

13

Since the V norm SV is characterized by relatively larger tropospheric perturbations than its E norm counterpart and tropospheric agreement between nonlinearly and tangent linearly evolved perturbations appears more problematic, the above comparison was repeated for the V norm SV. Its initial magnitude was also produced using a scaling of 0.1 applied to the original SV. This scaling yields initial maximum absolute values of u', v', and T' equal to 1.8 ms^{-1}, 1.9 ms^{-1}, and 3.1 K, respectively. These values occur near the surface and are much smaller than those in the previous experiment.

Results for the V norm experiment appear in Figs. 11 and 10b (analogous to Figs. 9 and 10a, respectively). Note the apparently strong correlations and similar magnitudes appearing in the 2 pairs of corresponding fields in Fig. 11. Correlations (Fig. 10b) are above 0.5 for all fields at levels in the stratosphere, with the wind correlations greater than 0.8 at several levels. Within the stratosphere at the final time, the nonlinear results have the maximum absolute magnitudes of u', v' and T' equal to 30 ms^{-1}, 27 ms^{-1} and 22 K, respectively. The better stratospheric agreements in this experiment may be due to these magnitudes being smaller than in the previous one, although they are still quite large. As in the previous experiment, the tangent linear and nonlinear tropospheric results are poorly correlated, although unlike in that experiment, their mean squared values are similar. Although the V–norm SVs are at least initially driven by tropospheric perturbations, the lack of tropospheric correlation obtained by day 5 of its evolution apparently has had little detrimental affect on the stratospheric agreement.

Agreement between nonlinear and tangent linear results above the troposphere depends on how well the sponge is tuned. In the experiments here, only a gross tuning was performed. In an earlier, developmental set of experiments, the sponge coefficients were so large as to damp almost all perturbations within the stratosphere. For the experiments reported here, those coefficients were therefore radically reduced within the lower strato-

sphere to the magnitudes reported in section 2. No change of the functional form of the coefficients was attempted, however, and it was deemed more important to ensure that numerically spurious structures do not appear near the upper boundary than to obtain a better match between the tangent linear and nonlinear results.

The 5–day period over which the SVs have been evolved here is longer than linearity typically holds for leading tropospheric SVs having the magnitude of initial condition uncertainty (Reynolds and Errico, 1999). Since the E norm growth factors for the stratospheric SVs are much smaller than for leading tropospheric ones, the extended linear applicability is not so surprising. What remains surprising is that the linearity holds even for the large initial magnitudes applied here. Smaller perturbations should yield at least as good agreement between tangent linear and nonlinear results unless the perturbation magnitudes are specified to be so small such that missing tangent linear physical parameterizations rather than nonlinear dynamics become the major source of disagreement. For reasons stated earlier, it is difficult to generalize the applicability of these SVs, especially without a specific objective for their use. Even so, the limited results here suggest that SVs having large initial amplitude may adequately describe nonlinear stratospheric perturbations out to 5 days.

8.   Conclusion

Only three SVs were described in detail here. These were all leading SVs for 5–day periods in January 2006, defined using the same final–time norm but for two different, but related, initial norms. SVs were computed for several other 5–day periods for the initial E norm and for both 2– and 5–day periods for the initial V norm. The latter periods included summer as well as winter ones. The first several leading SVs were computed for each period. The qualitative results reported here appeared to generally apply to all these

other SVs as well.

These stratospheric SVs have both notable similarities and differences compared with their typical tropospheric counterparts. Singular values are much larger in the winter, compared with summer, hemisphere. Perturbation shapes change strongly in time. Rotational winds strongly dominate divergent ones. The initial E norm SVs exhibit a strong eastward tilt as height increases, which becomes less pronounced as the SV evolves in time.

One important difference compared with their E–norm tropospheric counterparts is that, for periods of the same duration, singular values for stratospheric SVs are much smaller. This conclusion is based both on unpublished studies of E–norm tropospheric SVs with the same NASA adjoint model and with published results for tropospheric spectral models. Low resolution (e.g., T21L19), short period (e.g., 36 hour), SVs computed by considering only dry tangent linear dynamics and simple physics yield leading singular values of less than 7 for non–summer cases (Buizza at al., 1997; Palmer et al., 1998; Reynolds et al., 2001), and much higher values for longer periods, higher resolution, and more complete physics (Errico et al., 2004). Here the largest E norm singular value for 5 days during the winter season averaged less than 8.

The stratospheric SVs are also geographically (horizontally) less local than typical tropospheric ones. This result is not due to a lack of convergence by the Lanczos algorithm, which often explains any nonlocalness obtained for tropospheric SVs. Rather, it was shown to be due to the correlations that can develop from initially disparate SV structures: Initially distant and therefore distinct perturbation structures can yield remarkably similar perturbation structures by day 5. A linear combination of those distinct structures is therefore optimal when quadratic norms are applied at both initial and final times.

The vertical distribution of E for the SVs at both initial and final times was shown to

be very sensitive to the vertical weighting implied by the initial norm used to constrain the initial perturbations. Specifically, the usual, fractional mass ($\Delta\sigma$) vertical weighting employed in the perturbation energy (E) norm necessarily decays almost exponentially in stratospheric resolving models, such that initial perturbations in the troposphere are penalized much more strongly than in the stratosphere or above. This weighting therefore effectively precludes significant initial perturbations within the troposphere if any stratospheric perturbations themselves can produce significant E norm growth. Thus, unless it can be claimed that the E norm provides the most appropriate initial constraint, the result that initial, leading SV perturbations are confined to the stratosphere may be revealing more about the constraining norm itself than about atmospheric dynamics.

For the above reason, a norm that is like E but with an approximate fractional volume (V) weighting in the vertical was introduced. This norm produced SV structures with vertical partitionings of E at initial and final times dominated by the troposphere. Remarkably, however, the shapes of the corresponding horizontal structures of each dynamic field at each model level are highly correlated for the 2 different norms. Thus, the V norm primarily changes the relative scaling of perturbations at different model levels rather than entirely reshaping the structures.

If initial perturbations having the structure of tropospheric SVs and the amplitude of initial condition uncertainty (e.g., a local maximum of 3 ms^{-1} in wind and 1 K in temperature) are introduced in a nonlinear weather forecast model, after two days both the shapes and amplitudes of the perturbations will significantly depart from counterparts evolved using a tangent linear model (Reynolds and Rosmond, 2003; Errico and Raeder 1999). For the stratospheric SVs here, qualitative agreement between nonlinear and tangent linear evolutions was obtained for as long as 5 days. This was true for SVs initially dominated either by stratospheric perturbations (as constrained by an initial E norm) or

by tropospheric perturbations (as constrained by an initial V norm), with both having even larger initial and final magnitudes than in reported tropospheric experiments. So, these stratospheric SV structures are relevant in the nonlinear context. This relevance is aided by the facts that compared to the troposphere, highly nonlinear, moist precipitation physics is not very important in the stratosphere and singular values are smaller so that amplitudes do not become unrealistically large.

Leading stratospheric SVs potentially can be used to explain observed dynamical behaviors concerning the stratosphere. Their corresponding singular values, although generally smaller than their tropospheric counterparts, indicate significant growth. For suitable norms, tropospheric interactions are highlighted. For perturbation magnitudes of interest, the tangent linear results that define the SVs apply to the nonlinear context as well. Thus these SVs appear both interesting and relevant.

Acknowledgments

List of references

Andrews, D.G., J.R. Holton, C.B. Leovy, 1987: *Middle Atmosphere Dynamics.* – Academic Press, 489 pp.

Buizza, R., R. Gelaro, F. Moltani, T.N. Palmer, 1997: The impact of increased resolution on predictability studies with singular vectors. –Quart. J. Roy. Meteor. Soc. **123**, 1007–1033.

Buizza, R., T.N. Palmer, 1995: The singular vector structure of the atmospheric general circulation. –J. Atmos. Sci. **52**, 1434–1456.

Ehrendorfer, M., R.M. Errico, 1995: Mesoscale predictability and the spectrum of optimal perturbations. –J. Atmos. Sci. **52**, 3475–3500.

Errico, R.M., 1997: What is an adjoint model. Bull. Am. Meteor. Soc. **78**, 2577–2591.

Errico, R.M., 2000a: Interpretations of the total energy and rotational energy norms applied to determination of singular vectors. –Quart. J. Roy. Meteor. Soc. **126A**, 1581–1599.

Errico, R. M., 2000b: The dynamical balance of singular vectors in a primitive equation model. –Quart. J. Roy. Meteor. Soc., **126A**, 1601–1618.

Errico, R.M., K.D. Raeder, 1999: An examination of the accuracy of the linearization of a mesoscale model with moist physics. –Quart. J. Roy. Met. Soc. **125**, 169–195.

Errico, R.M., K.D. Raeder, M. Ehrendorfer, 2004: Singular Vectors for Moisture Measuring Norms. –Quart. J. Roy. Met Soc. **130A**, 963–988.

Errico, R.M., T. Vukićević, K. Raeder, 1993: Examination of the accuracy of a tangent linear model. –Tellus **45A**, 462–477.

Farrell, B.F., 1989: Optimal excitation of baroclinic waves. –J. Atmos. Sci. **46**, 1193–1206.

Gelaro, R., C. A. Reynolds, R.H. Langland, G.D. Rohaly, 2000: A predictability study using geostationary satellite wind observations during NORPEX. –Mon. Wea. Rev. **128**, 3789–3807.

Hoskins, B. J., R. Buizza, J. Badger, 2000: The nature of singular vector growth and structure. –Quart. J. Roy. Met. Soc. **126**, 1565–1580.

Lewis, J., K.D. Raeder, R.M. Errico, 2001: Vapor flux associated with return flow over the Gulf of Mexico: A sensitivity study using adjoint modeling. –Tellus **53A**, 74–93.

Lin, S.–J., R. Rood, 1996: Multidimensional flux–form semi-Lagrangian transport schemes. –Mon. Wea. Rev. **124**, 2046–2070.

Palmer, T. N., R. Gelaro, J. Barkmeijer, R. Buizza, 1998: Singular vectors, metrics, and adaptive observations. –J. Atmos. Sci. **55**, 633–653.

Reynolds, C.A., R. Gelaro, J.D. Doyle, 2001: Relationship between singular vectors and transient features in the background flow. –Quart. J. Roy. Meteor. Soc. **127**, 1731–1760.

Reynolds, C., R.M. Errico, 1999. Convergence of singular vectors toward Lyapunov vectors. –Mon. Wea. Rev. **127**, 2309–2323.

Reynolds, C.A., T.E. Rosmond, 2003: Nonlinear growth of singular vector based perturbations. –Quart. J. Roy. Met. Soc. **129**, 3059–3078.

Talagrand, O., 1981: A study in the dynamics of four–dimensional data assimilation. –Tellus **33**, 43–60.
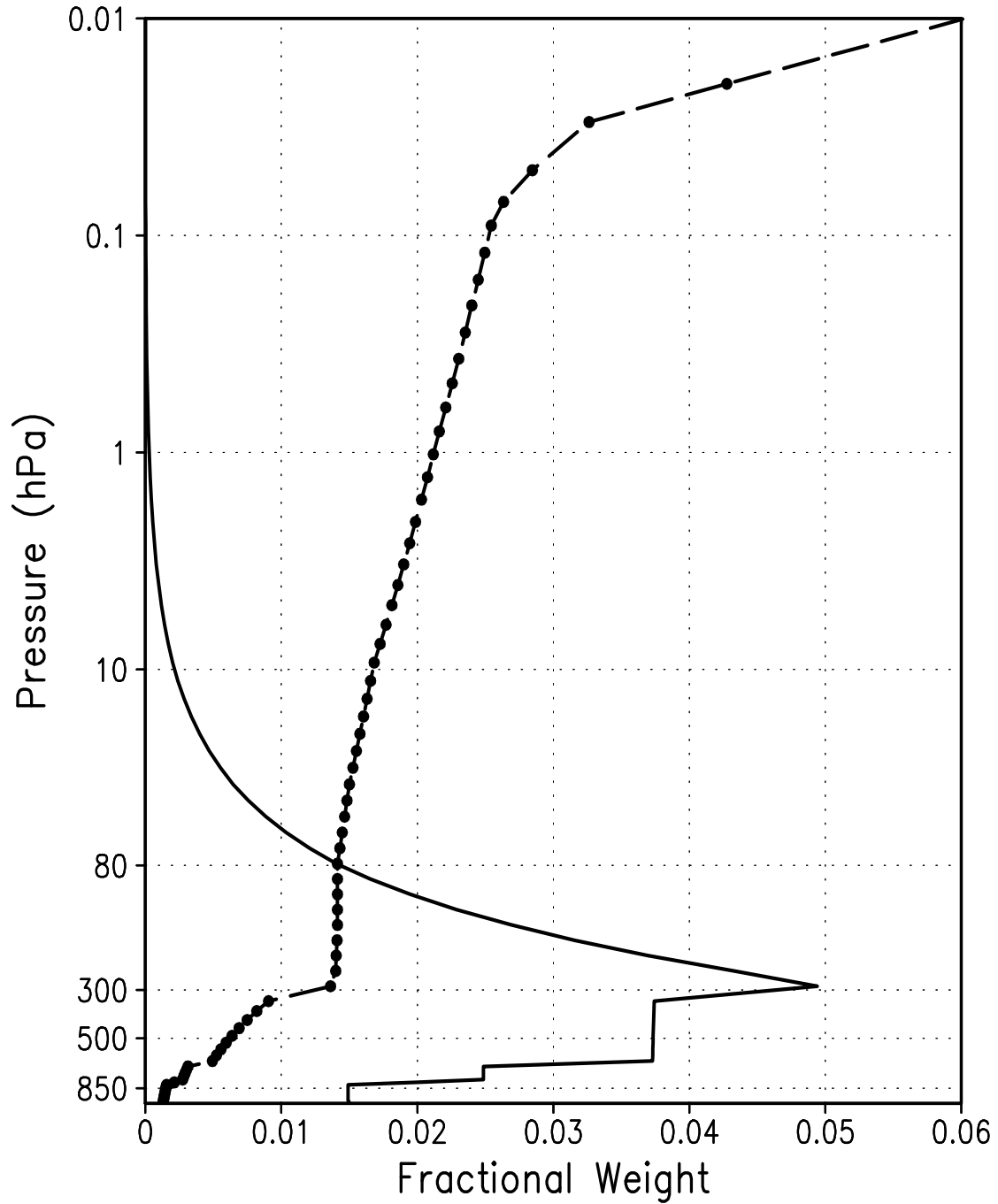
List of figure captions

Fig. 1. The fractional vertical weights $\Delta\sigma$ (solid) and Δz (dashed) used for calculating the E and V norms, respectively. The dots appearing on the dashed curve indicate the placement of model levels when $p_s = 1000$ hPa.
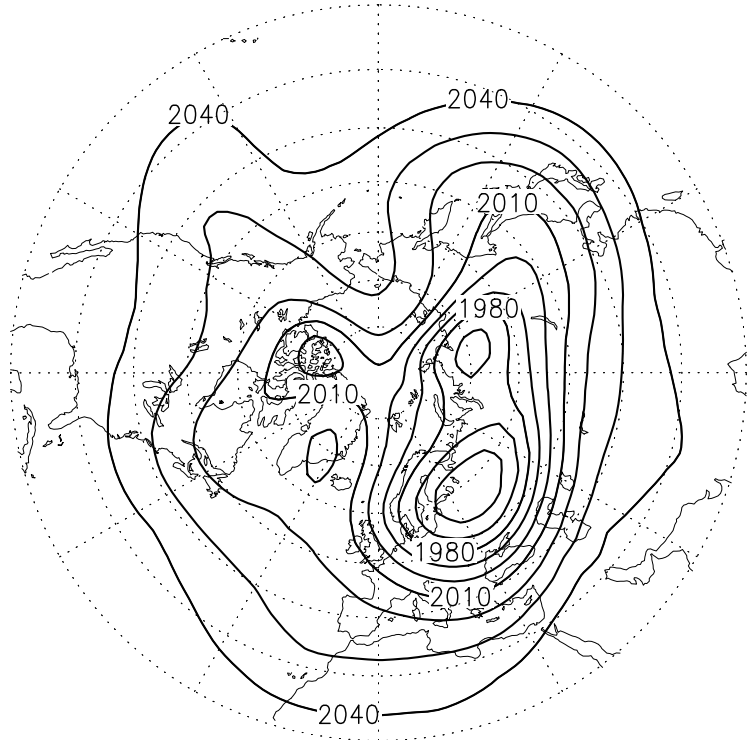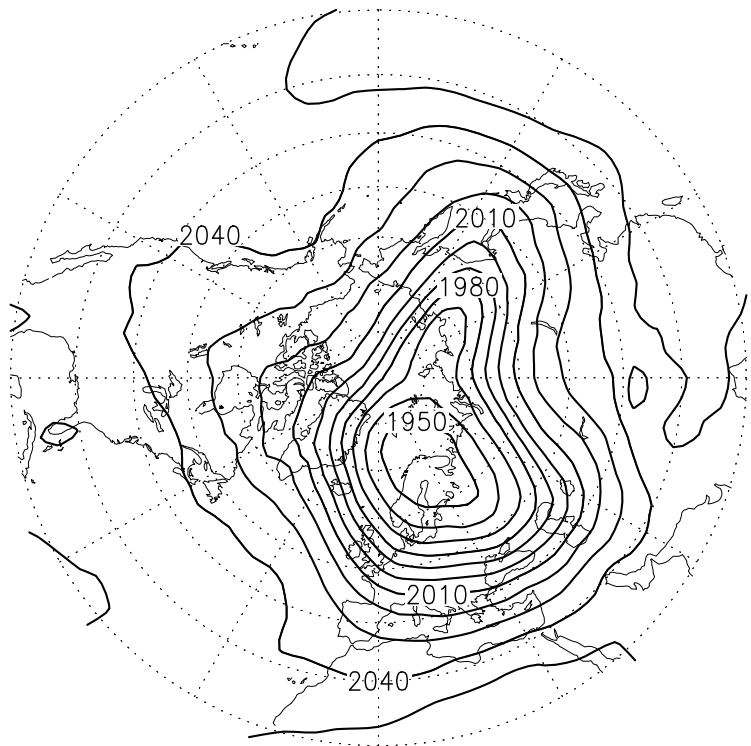
Fig. 2. The 50 hPa geopotential heights on (a) 21 January 2006 0UTC and (b) 26 January 2006 0UTC produced by the reference forecast for that period. Values are labeled in dm and the contour interval is 10dm.
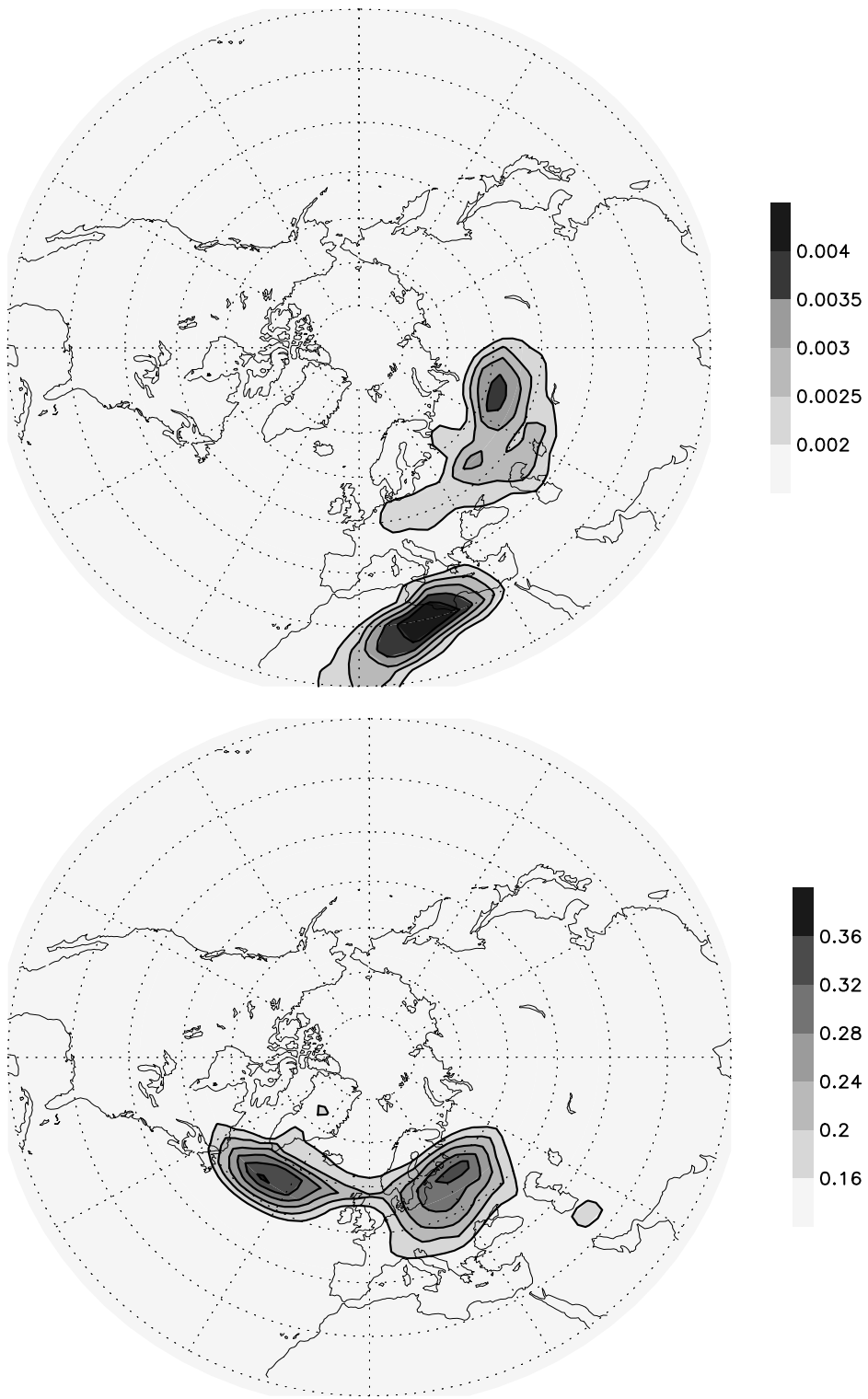
Fig. 3. The vertically integrated contribution to E for the leading SV for the focus period at (a) initial and (b) final times. Units indicating the shading are J/kg.

Fig. 4. The vertical distribution of (a) E for the focused, E norm SV at both initial (dashed) and final (solid times), presented as fractions of the total value of E and (b) the corresponding fractional energy densities.

Fig. 5. Cross section of v' through the stratosphere for the focused, E norm SV at (a) initial time along 60°N and (b) final time along 75°N. Units are in ms^{-1}.

Fig. 6. The vertically integrated contribution to initial E for the leading SV determined for the period 15–20 January 2006 appear in (a). Units are J/kg. The meridians for cutting the initial SV into 3 sectors are also shown in (a) with the sectors labeled 1–3. The u' field at 10 hPa for the tangent-linear, 5-day evolutions begun from the individual sectors 1–3 appear in (b–d), respectively. The shading is determined by absolute values, negative–valued contours are dashed, and units are ms^{-1}.
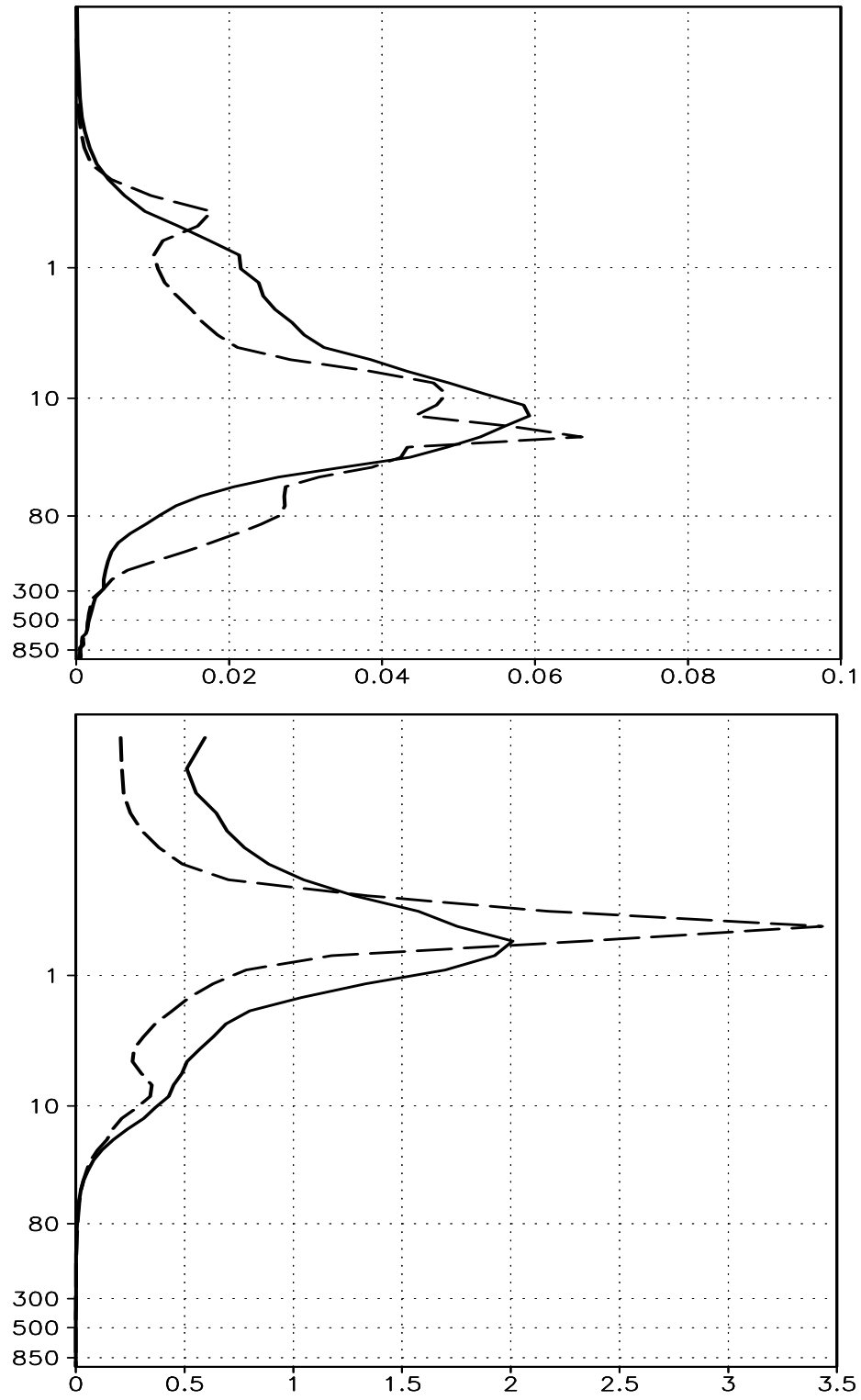
Fig. 7. The vertical distribution of (a) E for the focused, V norm SV at both initial (dashed) and final (solid times), presented as fractions of the total value of E and (b) the

corresponding fractional energy densities.

Fig. 8. The horizontal correlations of the corresponding E and V norm fields at individual model levels of u' at (dotted line) initial and (open circles) final times and for T' at (solid line) initial and (closed squares) final times. The correlations have been computed globally.

Fig. 9. Linearly (a,b) and nonlinearly (c,d) evolved perturbations at day 5 determined by an initial perturbation given by the initial-time, leading E norm SV for the focus period, with amplitude scaled by a factor of 0.1. The fields are (a,c) u' at 10 hPa, with units ms^{-1}. and (b,d) T' at 50 hPa, with units K. The shading is determined by absolute values, and negative-valued contours are dashed,

Fig. 10. The horizontal correlations of corresponding linearly and nonlinearly evolved, day–5 perturbations for the (a) E and (b) V norm SVs for u' (open circles), v' (closed squares) and T' (thin solid line) fields. The correlations have been computed globally.

Fig. 11. As in Fig. 9, except for the leading V norm SV for the focus period.

Figure 1: The fractional vertical weights $\Delta\sigma$ (solid) and Δz (dashed) used for calculating the E and V norms, respectively. The dots appearing on the dashed curve indicate the placement of model levels when $p_s = 1000$ hPa.

Figure 2: The 50 hPa geopotential heights on (a) 21 January 2006 0UTC and (b) 26 January 2006 0UTC produced by the reference forecast for that period. Values are labeled in dm and the contour interval is 10dm.   26

Figure 3: The vertically integrated contribution to E for the leading SV for the focus period at (a) initial and (b) final times. Units indicating the shading are J/kg.
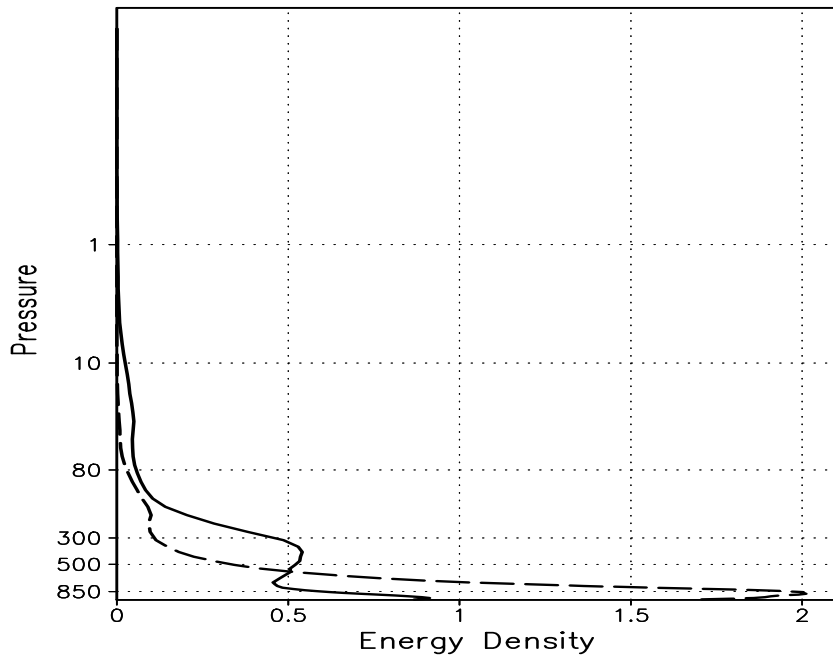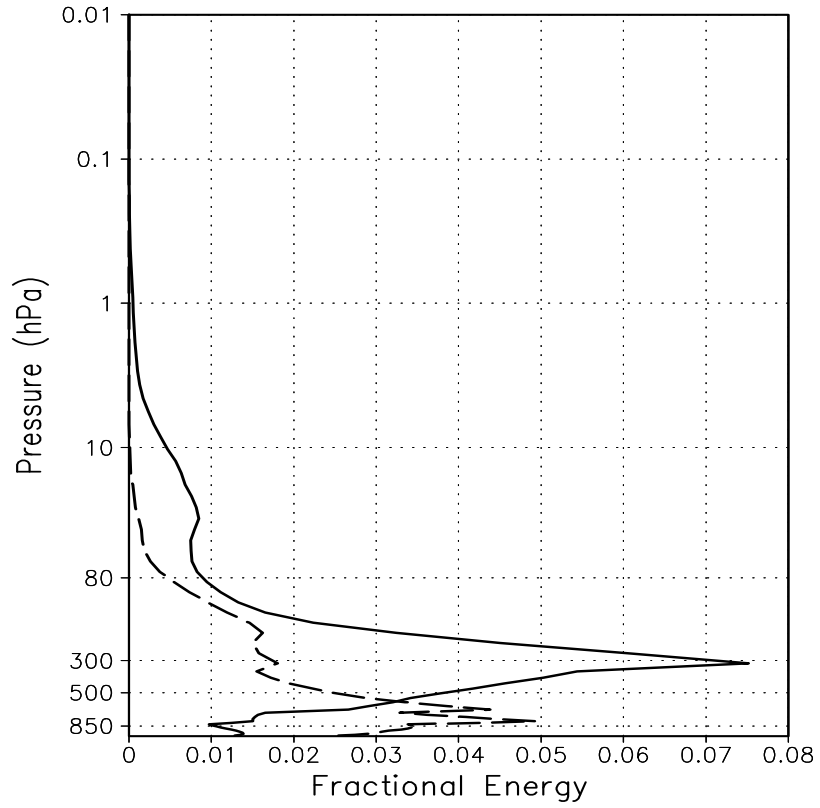
Figure 4: The vertical distribution of (a) E for the focused, E norm SV at both initial (dashed) and final (solid times), presented as fractions of the total value of E and (b) the corresponding energy densities.

28
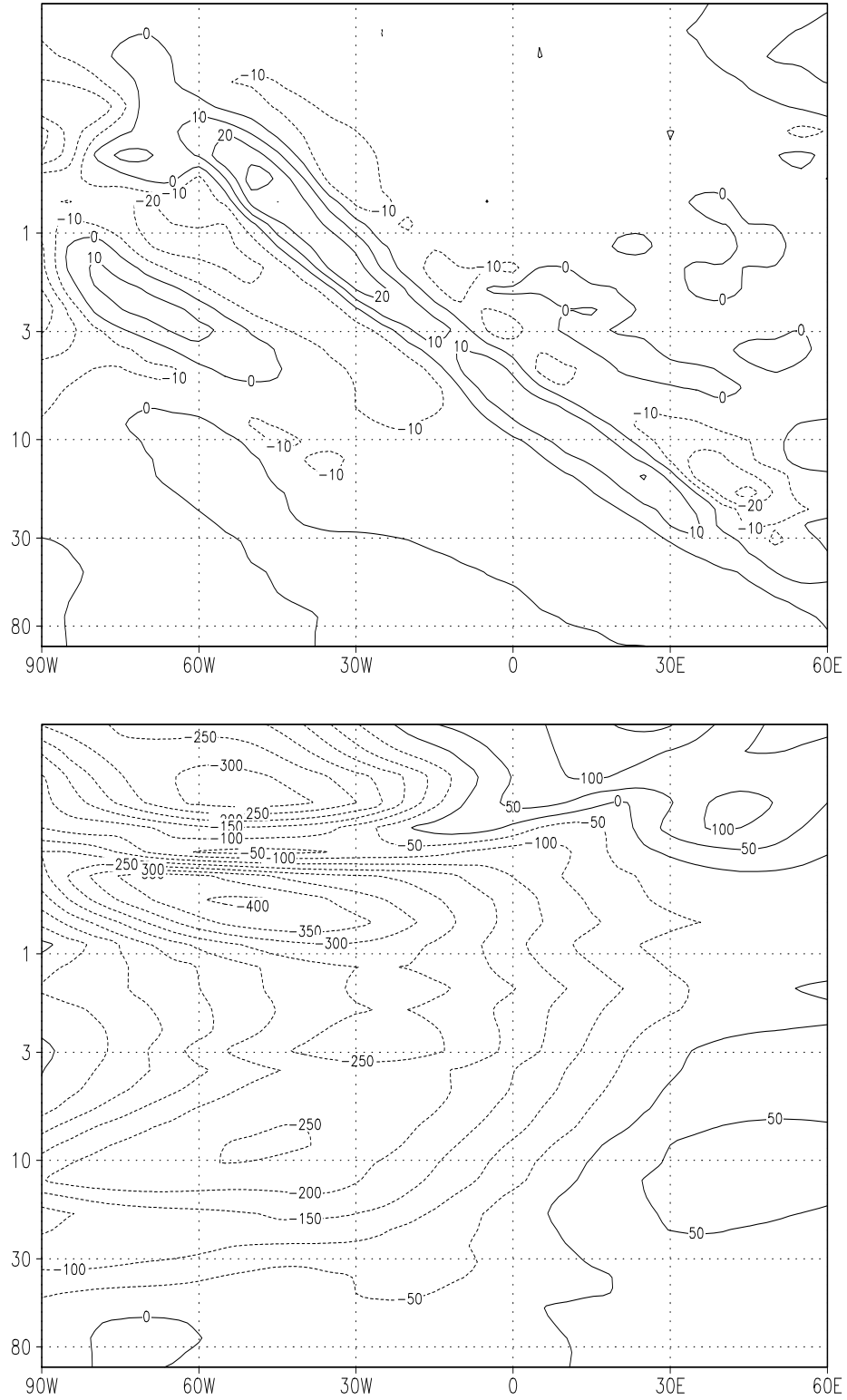
Figure 5: Cross section of v' through the stratosphere for the focused, E norm SV at (a) initial time along 60°N and (b) final time along 75°N. Units are in ms^{-1}.
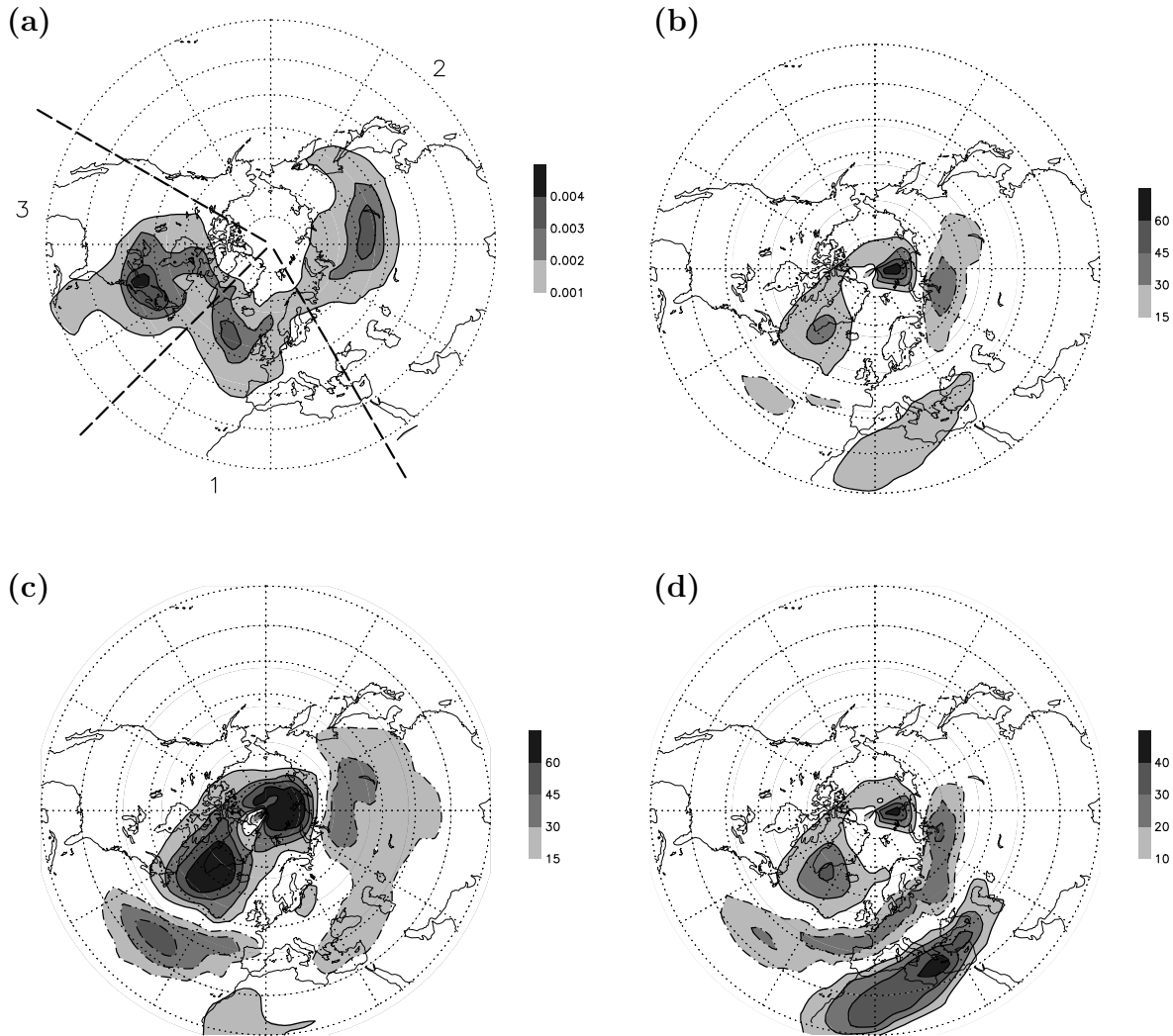
Figure 6: The vertically integrated contribution to initial E for the leading SV determined for the period 15–20 January 2006 appear in (a). Units are J/kg. The meridians for cutting the initial SV into 3 sectors are also shown in (a) with the sectors labeled 1–3. The u' field at 10 hPa for the tangent-linear, 5-day evolutions begun from the individual sectors 1–3 appear in (b–d), respectively. The shading is determined by absolute values, negative–valued contours are dashed, and units are ms^{-1}.

Figure 7: The vertical distribution of (a) E for the focused, V norm SV at both initial (dashed) and final (solid times), presented as fractions of the total value of E and (b) the corresponding energy densities. dashed curve in a is factor of 2 large.
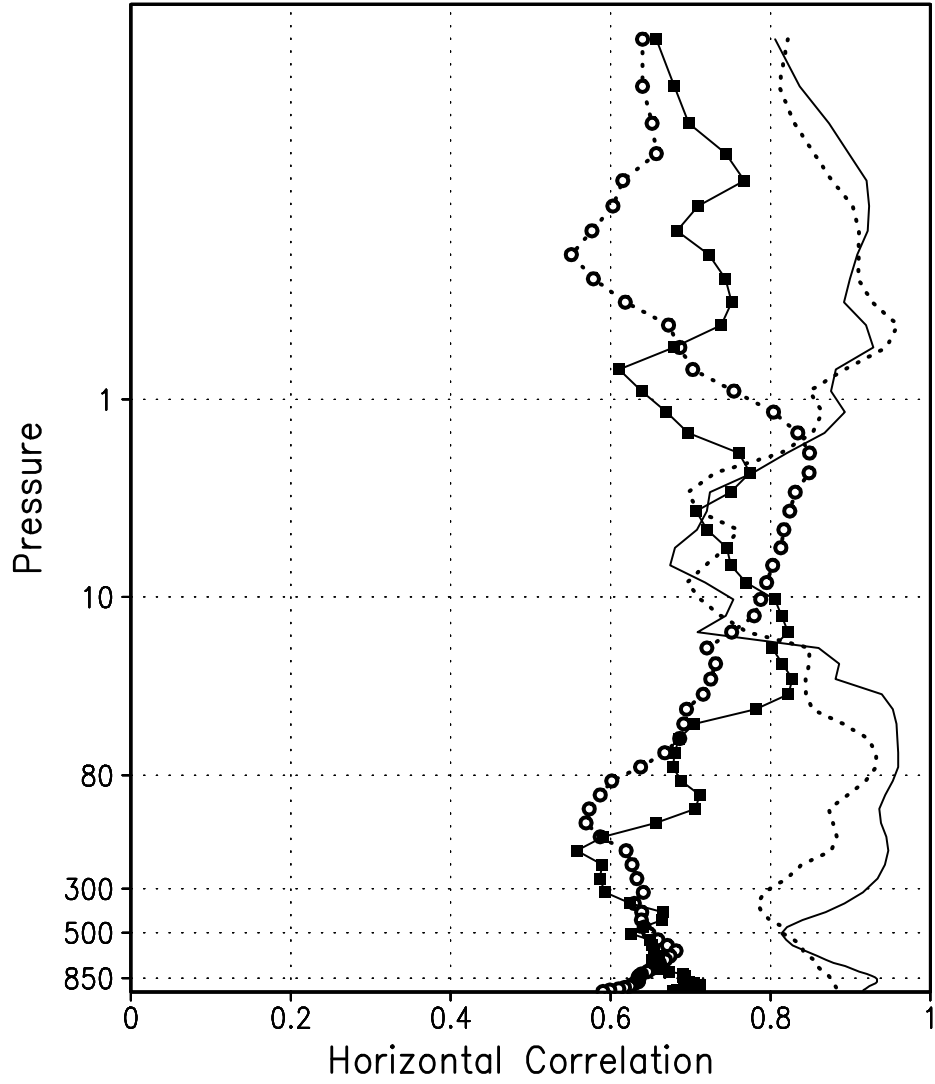
Figure 8: The horizontal correlations of the corresponding E and V norm fields at individual model levels of u' at (dotted line) initial and (open circles) final times and for T' at (solid line) initial and (closed squares) final times. The correlations have been computed globally.
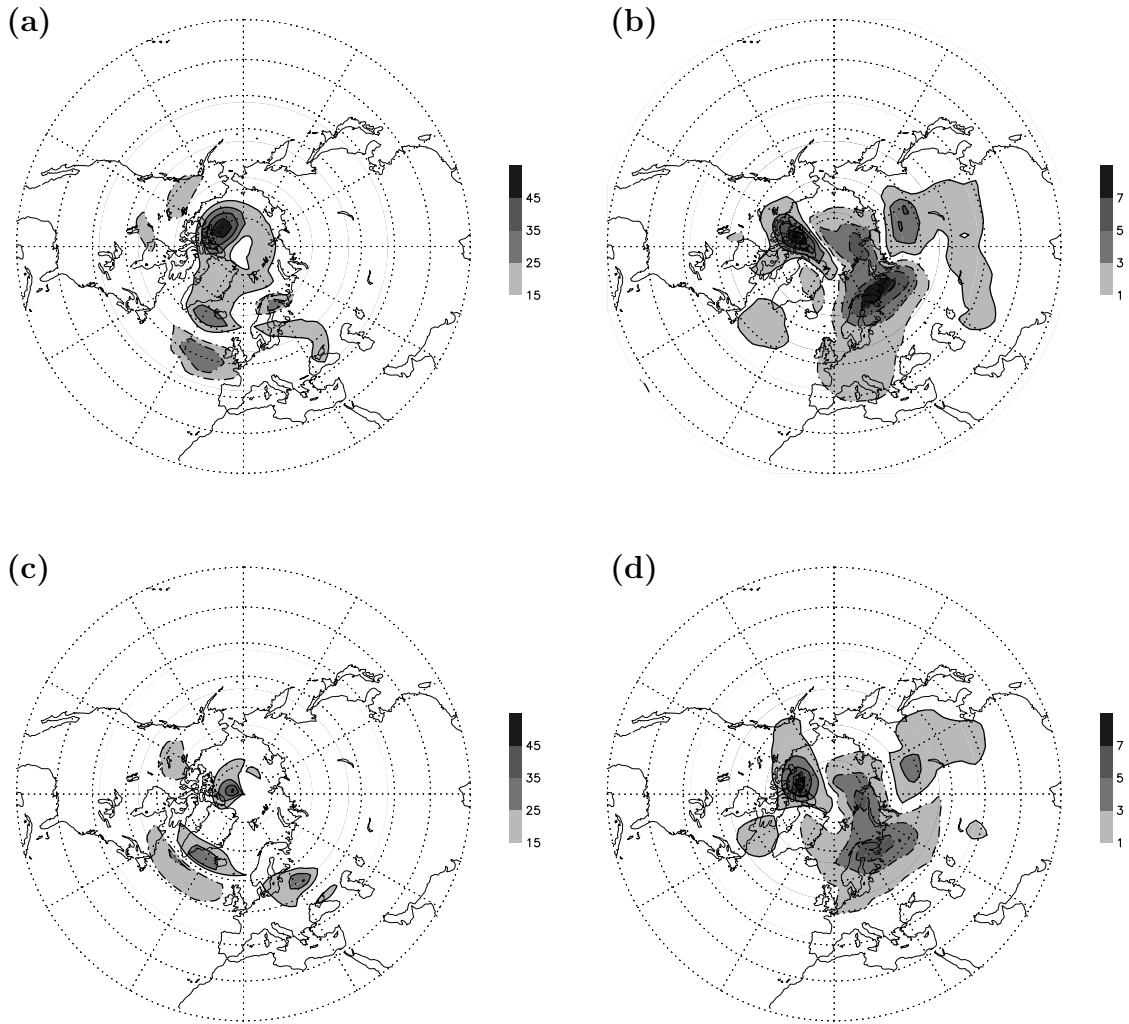
Figure 9: Linearly (a,b) and nonlinearly (c,d) evolved perturbations at day 5 determined by an initial perturbation given by the initial-time, leading E norm SV for the focus period, with amplitude scaled by a factor of 0.1. The fields are (a,c) u' at 10 hPa, with units ms^{-1}. and (b,d) T' at 50 hPa, with units K. The shading is determined by absolute values, and negative-valued contours are dashed.
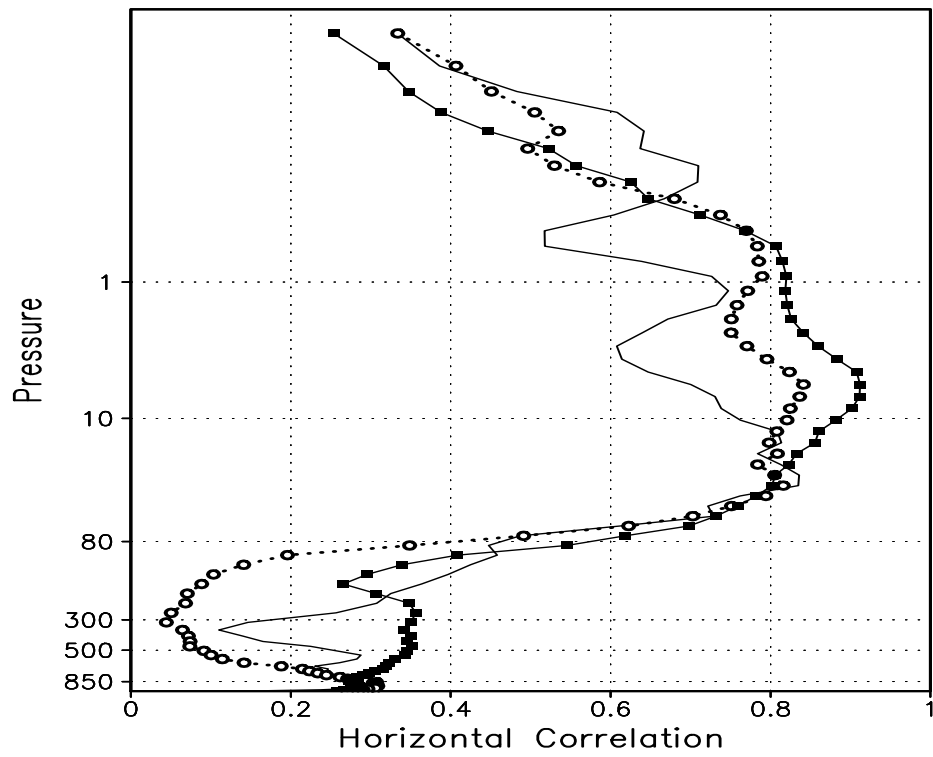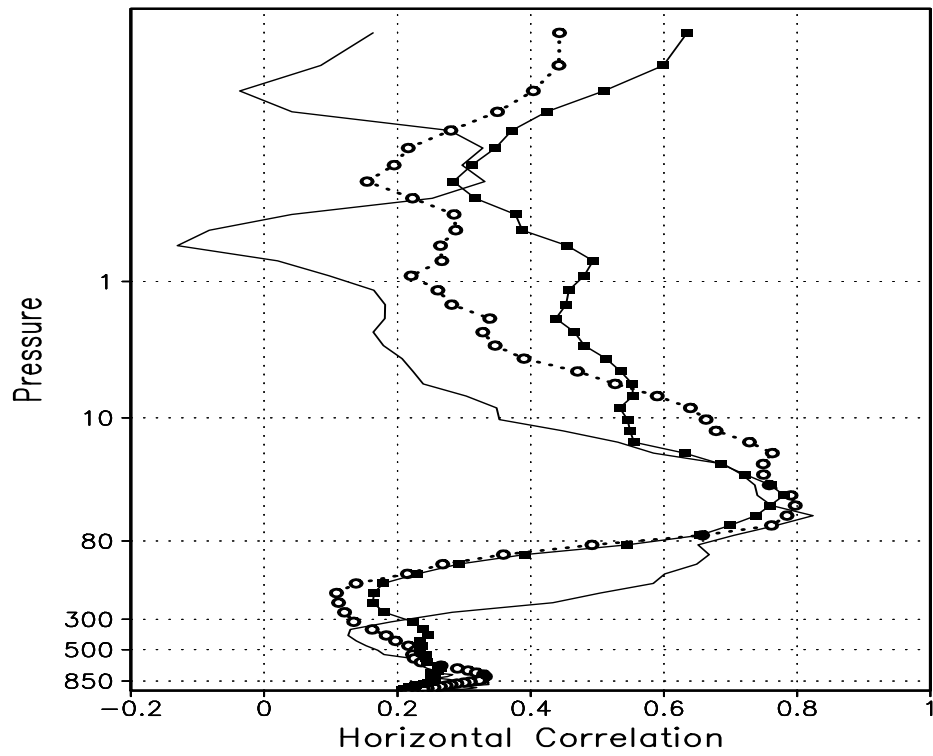
Figure 10: The horizontal correlations of corresponding linearly and nonlinearly evolved, day 5 perturbations for the (a) E and (b) V norm SVs for u' (open circles), v' (closed squares) and T' (thin solid line) fields. The correlations have been computed globally.
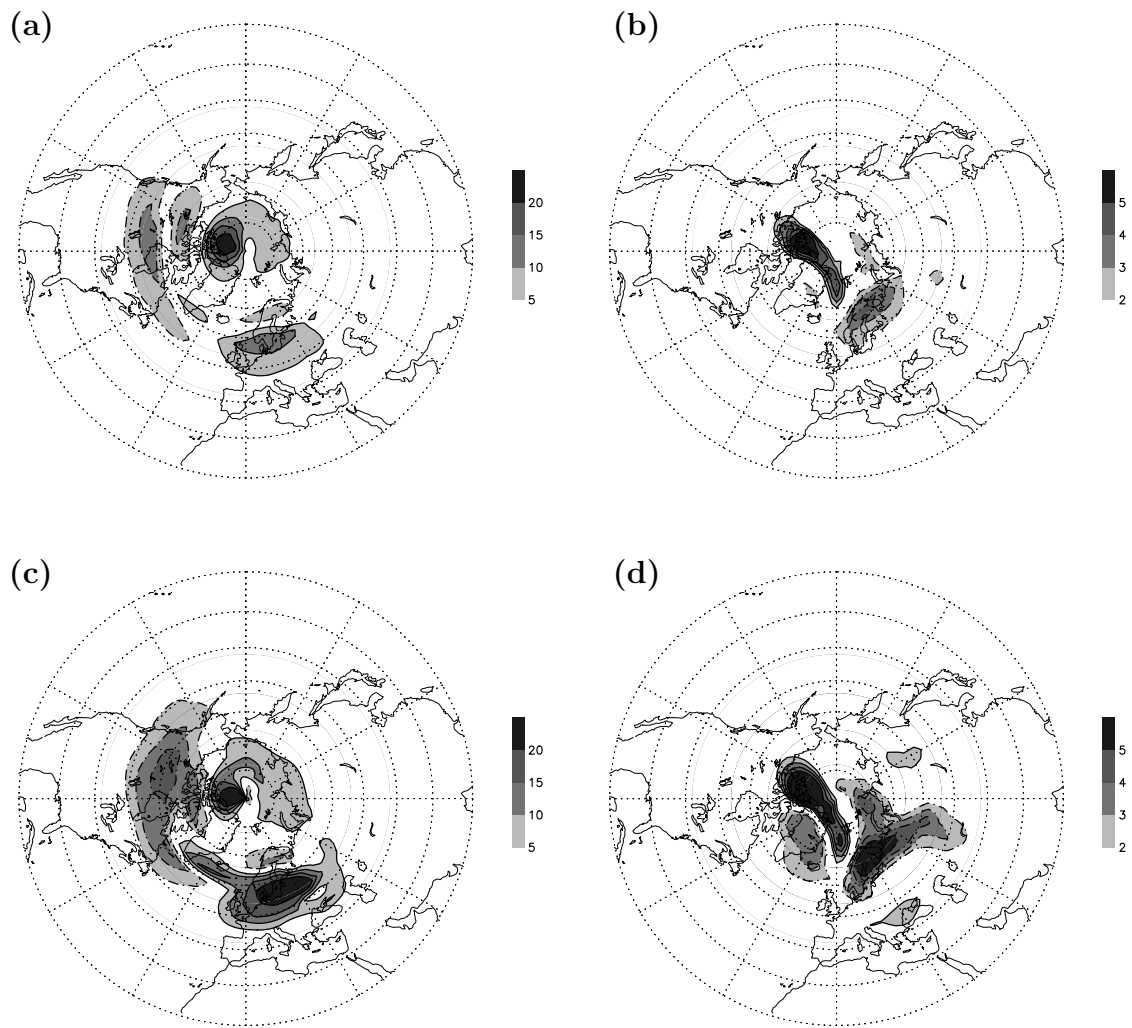
Figure 11: As in fig. 9, except for the V norm SV.